Hysteresis identification and dynamic responses of the impact drive mechanism

Jih-Lian Ha[a], Rong-Fong Fung[b],*, Chung-Shiang Yang[b]

[a]*Department of Mechanical Engineering, Far East College, 49 Chung-Hua Road, Shin-Shi, Tainan, Taiwan 744, ROC*
[b]*Department of Mechanical and Automation Engineering, National Kaohsiung First University of Science and Technology, 1 University Road, Yenchau, Kaohsiung 824, Taiwan*

Abstract

The main objective of this paper is to identify the hysteresis effect of a piezoelectric element (PE) and show its influence on the impact drive mechanism (IDM) which is a piezoelectric actuator (PA). As the IDM takes action due to the piezoelectric force, a Leuven model of the frictional force is proposed to modify the dynamic equations. For completely realizing the dynamic model, an adaptive identification method is quoted to experimentally identify the hysteresis parameters of the Bouc–Wen model. Moreover, a feedforward compensator is designed to make reparation the loss force of the PE due to nonlinearity of the hysteresis effect. Finally, simulation results of our compensator and the designed voltage waveforms are taken as the input commands to validate the excellent tracking performances of the IDM.
© 2004 Elsevier Ltd. All rights reserved.

1. Introduction

In the high-precision industry, the requirement of a micro/nano positioning system is getting more and more compulsory. The PA has been widely used in a positioning system because the PE has the characteristics of good performances in the controlling of precise motion, high-frequency response, high electrical mechanical coupling efficiency, small size, and small thermal expansion

---

*Corresponding author. Tel.: +886 7 601 1000x2221; fax: +886 7 601 1066.
E-mail address: rffung@ccms.nkfust.edu.tw (R.-F. Fung).

during actuation. The position accuracy can possibly attain to 1–10 nm, but the total displacement of a piezoelectric actuator has only a few micrometers. To overcome this main disadvantage, a number of efforts have been made in the practical applications. In this paper, we are going to study the IDM, which is an actuation mechanism utilizing only one PE.

The development of the IDM began with the design of a finely adjustable specimen holder for the scanning tunneling microscope in the 1980s. Higuchi et al. [1–3] proposed a prototype IDM for the design of a micro robot that serves as an inserted capillary in a cell-operation. Furutani et al. [4] studied the effect of lubrication on the IDM, and discussed the motion of the IDM based on the Newtonian mechanics. An approximate estimation of the IDM motion under a specific exciting waveform pattern was provided. It was found that surface condition did not apparently affect the behaviors of the IDM, and the stick-slip operation was dominated by energy dissipation of the frictional force between the slider and the guide surfaces. Recently, Liu et al. [5,6] have presented a simple mechanical vibration model to analyze the dynamic characteristics of the precision positioning table utilizing a spring-mounted piezoelectric actuator.

The first focus of this paper is to build the dynamic equations of the IDM with the nonlinear hysteresis behavior of a piezoelectric actuator and the frictional effect due to the contact between the sliding surface and the main body. The hysteresis effect is based on the differential equation of the Bouc–Wen model, while the frictional force is adopted by the Leuven model [7]. After constructing the dynamic equations of the IDM, the identified skill of the nonlinear hysteresis behavior and a feedforward compensator to compensate the hysteresis effect are introduced to improve the accuracy of the IDM.

2. Physical system

The configuration of the IDM system is shown in Fig. 1. It includes a main body m_1, a weight m_2 and a PE. The main body is attached to the right-hand side of the PE and always keeps moving in the x-axis by a fixed sliding track. The weight is attached to the left-hand side of the PE, and it does not contact with the sliding surface. In Fig. 1(a), the forward motion of the IDM can be separated as four parts: (1) start at original state; (2) a rapid extension of the PE as given the PE rapid extensional voltage waveform; (3) contracted the PE slowly to keep the main body hold its position by frictional force; and (4) suddenly stop the input voltage to achieve the second forward movement. Repeating these four steps, the main body could move forward in infinite distance through these step-like movements. The backward motion shown in Fig. 1(b) can be made by exchanging extensions with contractions of the above steps.

3. Dynamic formulation

3.1. The dynamic equations of the IDM

The schematic diagram of the IDM is shown in Fig. 2(a), and its free-body diagram is shown in Fig. 2(b), where x_1 and x_2 are the coordinates to describe the main body and the weight, respectively. The PE can be regarded as an equivalent spring, denoted as k_p, and a viscous
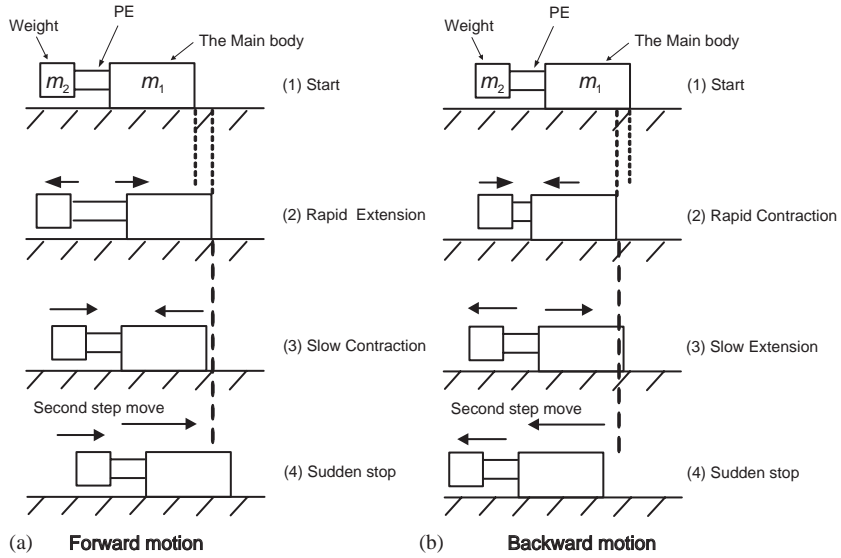
Fig. 1. Physical system of the IDM: (a) forward motion; (b) backward motion.
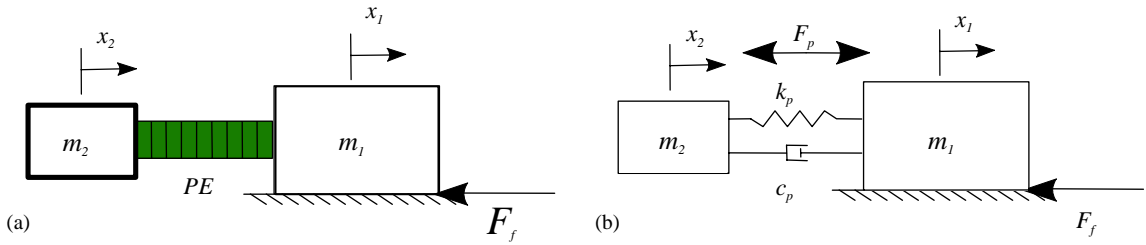

Fig. 2. The system diagram of the IDM: (a) schematic diagram of the IDM model: (b) the free-body diagram of the IDM for theoretical analysis.

damping, denoted as c_p. The piezoelectric force is $F_p = E_P d_{33} A_P V / l$ [8], where E_P is its Young's Modulus, d_{33} is its piezoelectric coefficient, A_P is its cross-section area, l is its length, and V is the input voltage. The frictional force F_f appears between the main body and the sliding surface. By using Newton's second law, the governing equations are easily obtained as follows:

$$m_1 \ddot{x}_1 + c_p(\dot{x}_1 - \dot{x}_2) + k_p(x_1 - x_2) = F_p - F_f, \tag{1a}$$

$$m_2 \ddot{x}_2 + c_p(\dot{x}_2 - \dot{x}_1) + k_p(x_2 - x_1) = -F_p. \tag{1b}$$

3.2. Hysteresis model

Fig. 3 plots a typical hysteresis loop between the input and output signals. In order to solve these kinds of nonlinear problems, there have been tremendous amounts of research efforts about modeling hysteresis [9–12] in the past. The modified Preisach's model [9] provides the ability to

predict the minor loop behavior of piezoelectric actuators by using the additional measured data of second-order reversal curves. But it increases the complexity of algorithms and the number of stored datasets, therefore such a model is not suitable for controller design purposes. Goldfarb and Celanovic [10] used a generalized Maxwell resistive capacitor as a lumped-parameter causal representation of rate-independent hysteresis. In contrast with the infinite number of hysteresis operators, which were used to construct the nonlinearity of hysteresis in Preisach's model, a finite number of Maxwell slip elements connected in parallel can effectively describe nonlinearity of hysteresis. However, we have to decide the number of Maxwell slip elements through experiments. It makes the system become undefined.

In this paper, the operating principle of the IDM is based on a repeating designed input voltage waveform, and the hysteresis model for the PE adopts a simple Bouc–Wen model [11], which presents a differential equation describing the hysteresis model with only three parameters:

$$\dot{z} = A\dot{u} - \beta|\dot{u}|z|z|^{n-1} - \gamma\dot{u}|z|^{n}, \tag{2}$$

where the parameters A β and γ control the shape of the hysteresis loop, and n is an integer. Eq. (2) is a first-order nonlinear differential equation, which represents the hysteretic relationship between the state variable z and the excitation $\dot{u}$. It has been experimentally modified that this differential equation is also suitable to describe the hysteresis phenomenon of the PA by Low and Guo [12]. The modified equation is shown as follows:

$$\dot{h} = \alpha d_{33}\dot{V} - \beta|\dot{V}|h - \gamma\dot{V}|h|, \tag{3}$$

where h is a state variable, d_{33} is the piezoelectric coefficient, and V denotes the input voltage.

In this paper, the frequency and the shape of input voltage waveform to the IDM is fixed, so that the first-order nonlinear differential Eq. (3) with only three parameters is very suitable to describe the symmetry hysteresis phenomenon and easily to design a controller. As we consider the hysteresis effect is a kind of energy dissipation of the PE, we can introduce the state variable h to the piezoelectric force F_P in Eq. (1). The modified dynamic equations of the IDM with
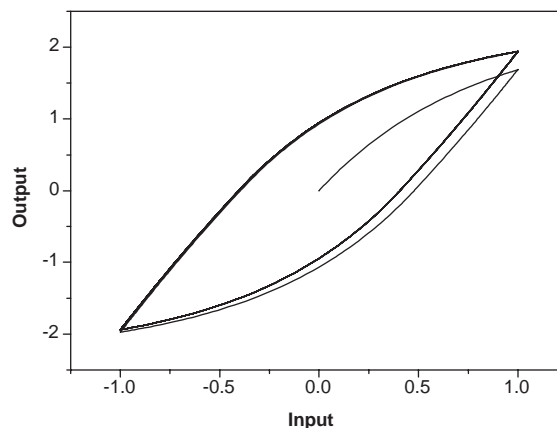

Fig. 3. The typical hysteresis phenomenon.

consideration of the hysteresis phenomenon are given as

$$m_1\ddot{x}_1 + c_p(\dot{x}_1 - \dot{x}_2) + k_p(x_1 - x_2) = (F_p - k_p h) - F_f, \tag{4a}$$

$$m_1\ddot{x}_1 + c_p(\dot{x}_1 - \dot{x}_2) + k_p(x_1 - x_2) = (F_p - k_p h) - F_f. \tag{4b}$$

Eqs. (3) and 4(a,b) construct the dynamic model of the IDM in consideration with the frictional force F_f between the main body and the sliding surface, and the nonlinear hysteresis property between the piezoelectric force F_P and the input voltage V. For selecting appropriate values of the parameters α, β and γ, we will introduce an adaptive identification process to design these parameters in Section 5.

3.3. Frictional force model

When two surfaces contact and have relative motions, frictional force exists and plays a dominant role in the motion behavior of the IDM. In the IDM, the frictional force will importantly decide whether or not the mechanism can work, thus using a proper model for the frictional force effect in the IDM will be necessary. In the above Eq. (4), the frictional force F_f is not yet defined.

A frictional force model that can incorporate presliding motion and the stick slip of mechanical parts with small applied forces is required to predict the behavior of the IDM with small input voltage. The Leuven model [13] allows a good description of the constant-velocity behavior to offers a smooth transition at velocity reversal, and has good performance in emulations of the presliding behavior in frictional contact. Fig. 4 plots a typical Leuven frictional force model which is combined from the Dahl model with arbitrary steady-state frictional characteristics of the Stribeck effect. The Leuven model contains a state variable of the averaged deflection of elastic bristles which are a visualization of the contacting surfaces. The Leuven model [13] is shown as follows:

$$\frac{dz}{dt} = v\left(1 - \text{sgn}\left(\frac{F_h(z)}{s(v)}\right)\left|\frac{F_h(z)}{s(v)}\right|^n\right), \tag{5a}$$

$$F_f = F_h(z) + \sigma_1\frac{dz}{dt} + \sigma_2 v, \tag{5b}$$

where z is the state variable, $F_h(z)$ represents a hysteresis function in the static frictional force, v is the velocity, n is a coefficient used to shape the transition curves and $s(v) = \text{sgn}(v)(F_c + (F_s - F_c)e^{-(|v|/v_s)^2})$ is a function that models the constant-velocity behavior, where F_c is Coulomb frictional force, F_s is the maximum static force and v_s is the Stribeck velocity. In Eq. (5b), σ_1 is the micro-viscous frictional coefficient, and σ_2 is the viscous frictional coefficient [7].

4. Experimental setup

Fig. 5(a) shows a photograph of the IDM, where the PE is produced by Tokin Company and has the dimensions of $5 \times 5 \times 20\,\text{mm}$. Fig. 5(b) shows the chart of the whole experimental setup. The designed waveforms of applied voltage are generated by the LabVIEW software. The
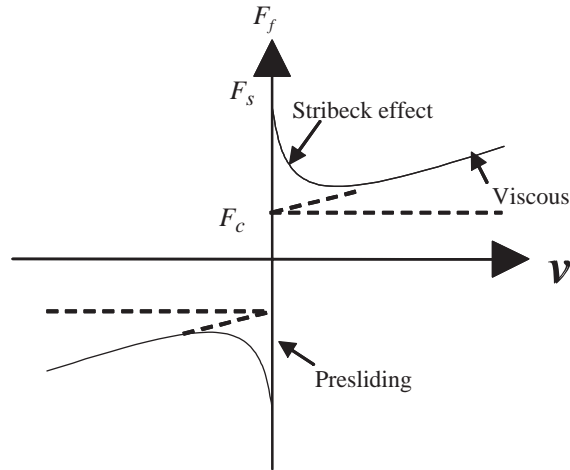
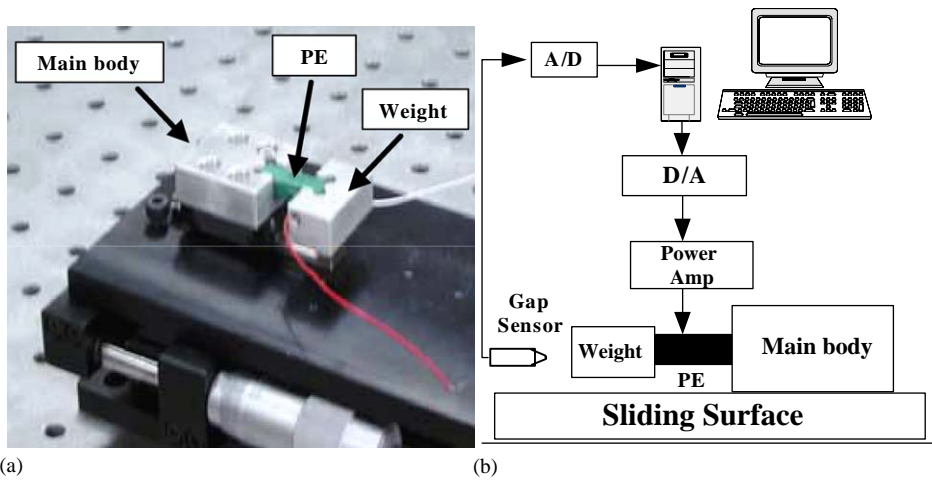Fig. 4. The typical Leuven frictional force model.

(a)　　　　　　　　　　　　　　　(b)

Fig. 5. Experimental setup: (a) photograph of the IDM; (b) configured experimental setup.

DA/AD converter (PCI-6052E) with a resolution of 12 bit is used to transform the input voltage to the power amplifier which has the voltage output range $\pm200\,\mathrm{V}$, and then send to the PE. A capacitor-type gap sensor (Micro Sense: 3401-RA2) with the measuring range $\pm25\,\mu\mathrm{m}$, and the corresponding resolution of 10 nm is used to precisely detect the motion the main body.

In this paper, we are interesting in the hysteresis effect of the PE in the motion of the IDM. There are three steps for constructing the identification experiments. First, the main body is fixed by a screw. Secondly, the designed input voltage waveform generated by the LabVIEW software is given to the PCI-6052E for the D/A conversion, passes through the power amplifier and activates the PE. Finally, the capacitor-type gap sensor is used to measure the displacement data for the hysteresis identification.

5. Hysteresis identification

Identification is the process of developing an accurate mathematical model for a system through set of given inputs and corresponding measured outputs. It is usually the first step taken by control engineers since the control requires complete understanding of the system before one tries to control it. For the PA, the identifications of the uncertain parameters in the hysteresis model are widely encounted, and much effort has been devoted by numerous investigators to identify such a hysteresis system [14–16]. Chassiakos et al. [17] proposed an efficient on-line identification method in the hysteresis system.

Fig. 6 shows the free-body diagram of the PA, in which the parameters of the hysteresis model (3) need to be identified. Consider the m_p as the equivalent mass of the PE plus the mass of the weight, one obtains the following dynamic equation:

$$m_p\ddot{x}_p + c_p\dot{x}_p + k_px_p = F_p - k_ph, \tag{6}$$

where c_p is the viscous damping, and k_p is the equivalent spring.

In this paper, the experiment measurements are taken at a discrete-time interval Δt, then the discrete-time version model of Eq. (3) is as follows:

$$h(k) = h(k-1) + \Delta t[\alpha d_{33}\dot{V}(k-1) - \beta|\dot{V}(k-1)|h(k-1) - \gamma\dot{V}(k-1)|h(k-1)|]. \tag{7}$$

The discrete-time estimator is expressed as follows:

$$\hat{h}(k) = h(k-1) + \phi^{\mathrm{T}}(k-1)\hat{\theta}(k), \tag{8}$$

where $\hat{h}(k)$ is the estimate state at time $t(k)$, $\phi^{\mathrm{T}}(k-1)$ is a vector combined by the experimental measurements $\dot{V}(k-1)$ and $h(k-1)$. The latter is calculated from Eq. (6) by using the measured data $x_p(k-1)$, $\dot{x}_p(k-1)$ and $\ddot{x}_p(k-1)$ at time $t(k-1)$. $\hat{\theta}(k)$ is the vector containing parameters α, β and γ, which are going to be identified.

Then using the following adaptation law [17]:

$$\theta(k) = \begin{cases} \mu(k) & \text{if } ||\mu(k)|| \leqslant M_\theta, \\ \left(\frac{M_\theta}{||\mu(k)||}\right)\mu(k) & \text{if } ||\mu(k)|| \geqslant M_\theta, \end{cases} \tag{9a}$$

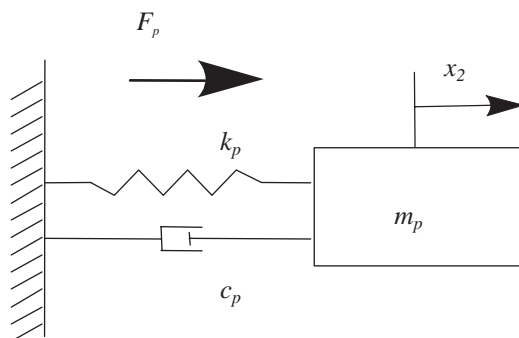

Fig. 6. The free-body diagram of the PA for theoretical analysis.

Table 1
Experimental setup for identification parameters of the Bouc–Wen model

Cross-section area of the PE	A_p	$2.5 \times 10^{-5} \, \text{m}^2$
Damping coefficient of the PE	c_p	$25 \, \text{Ns/m}$
Piezoelectric coefficient	d_{33}	$1.24 \times 10^{-7} \, \text{m/V}$
Young's modulus of the PE	E_p	$2.216 \times 10^{10} \, \text{N/m}^2$
Stiffness coefficient of the PE	k_p	$2.77 \times 10^7 \, \text{N/m}$
Length of the PE	l	$2 \times 10^{-2} \, \text{m}$
Equivalent mass of the PE plus the mass of the weight	m_p	$19.25 \times 10^{-3} \, \text{kg}$
Constant in the adaptation law	M_0	3
Constant in the adaptation law	β_0	1000
Constant in the adaptation law	γ_0	25

$$\mu(k) = \theta(k-1) - \frac{\gamma_0}{\beta_0 + \|\phi(k-1)\|^2} e(k-1)\phi(k-1), \tag{9b}$$

where γ_0 and β_0 are constants to speedy the converging time, $e(k-1)$ is the estimation error of $\hat{h}(k-1) - h(k-1)$, M_θ is a chosen constant to avoid parameter drift, which could drive the estimate $\hat{\theta}(k)$ to infinity. Eq. (9b) projects the vector $\mu(k)$ back onto the surface of a hypersphere of radius M_θ if $\mu(k)$ lies outside of this hypersphere. The adaptation law expressed by Eqs. 9(a,b) guarantees that all the signals will remain bounded [17].

Now we can identify the parameters α, β, and γ experimentally, by given the designed input voltage waveform to the PE. The experimental setups are listed in Table 1. The tracking results of this adaptive identification method are shown in Fig. 7(a)–(d). Fig. 7(a) shows the hysteresis phenomenon between the input voltage and the responses x_p. From the experimental results shown in Figs. 7(b)–(d), we obtain the identified parameters: $\alpha = 10$, $\beta = 0.06$ and $\gamma = -0.06$ for the Bouc–Wen model.

6. Numerical simulation

To solve the dynamic equations (3) and (4), the fourth-order Runge–Kutta method is implemented by Simulink which is a supported toolbox in windows type of Matlab. All the parameters used for calculations are listed in Table 2, where σ_1 and σ_2 are adopted from the experimental results [7], and the other parameters are coincident with the experimental setup.

Fig. 8 show the dynamic model simulations of the IDM. Fig. 8(a) shows the designed voltage waveform which has a constant slope for 0–0.5 ms and an ellipse function $(x - x_0)^2/a^2 + (y - y_0)^2/b^2 = 1$ for 0.5–3 ms, where $(x_0, y_0) = (0.5, 0)$ is the center of ellipse indicated by a black spot. The displacements of the main body with and without the hysteresis effects are compared in Fig. 8(b). The hysteresis behavior can be described as energy dissipation, and decreases the displacement. Fig. 8(c) is the nonlinear hysteresis phenomenon between the piezoelectric force
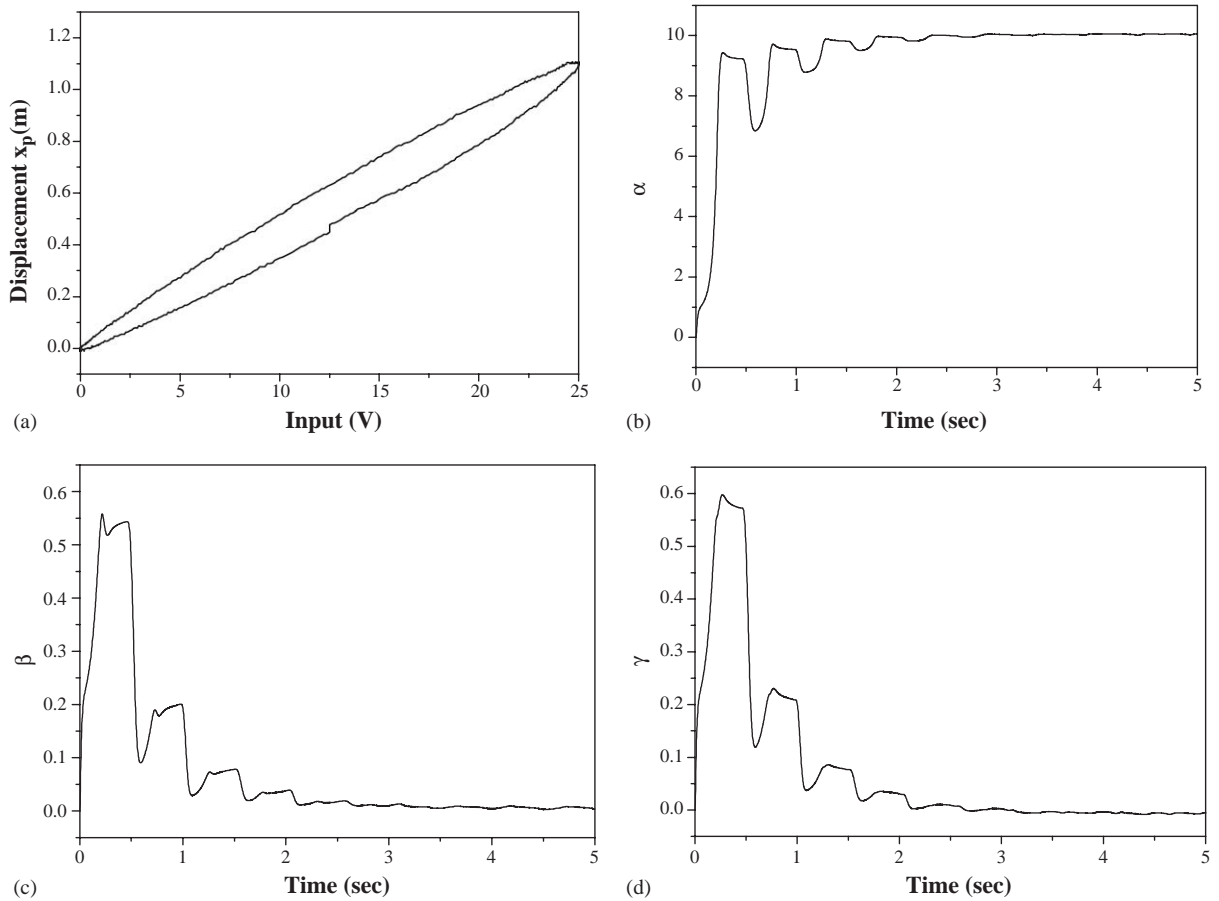
Fig. 7. Identification the parameters of the Bouc–Wen model: (a) hysteresis phenomenon between the input voltage and the response x_p. The tracking processes of (b) parameter α, (c) parameter β, and (d) parameter γ.

Table 2
Parameters in the numerical simulations of the IDM model

Cross-sectional area of the PE	A_p	$2.5 \times 10^{-5}\,\mathrm{m}^2$
Damping coefficient of the PE	c_p	$25\,\mathrm{Ns/m}$
Piezoelectric coefficient	d_{33}	$1.24 \times 10^{-7}\,\mathrm{m/V}$
Young's modulus of the PE	E_p	$2.216 \times 10^{10}\,\mathrm{N/m}^2$
Stiffness coefficient of the PE	k_p	$2.77 \times 10^{7}\,\mathrm{N/m}$
Length of the PE	l	$2 \times 10^{-2}\,\mathrm{m}$
Mass of the main body	m_1	$175.75 \times 10^{-3}\,\mathrm{kg}$
Mass of the weight	m_2	$15 \times 10^{-3}\,\mathrm{kg}$
Shape coefficient of the transition curves	n	1
Static frictional coefficient	μ_s	0.55
Dynamic frictional coefficient	μ_k	0.45
Micro-viscous frictional coefficient	σ_1	$300\,\mathrm{Ns/m}$
Viscous frictional coefficient	σ_2	$1\,\mathrm{Ns/m}$

F_P and the input voltage V. Fig. 8(d) shows the simulation results of the Leuven model of the frictional force model.

In Fig. 9(a)–(d), the advantages of different shapes of the input voltage waveform are compared for both the forward and backward motions. In Fig. 9(a) a new designed shape of the input voltage waveform with a quarter of ellipse is compared with a triangular input voltage waveform, which was often used in Refs. [18–20]. The two inputs have the same slope during 0–0.5 ms, but different shapes during 0.5–3 ms. Fig. 9(b) shows the main-body displacements for the two different shapes of the input voltages. It is found that the new designed input shape has better performance than that of the triangular one in the forward motion. Fig. 9(c) shows the triangular input voltage waveform compared with the new designed ellipse input voltage waveforms in the backward motion. Fig. 9(d) shows that the ellipse input voltage waveform has the better performance than that of the triangular one.
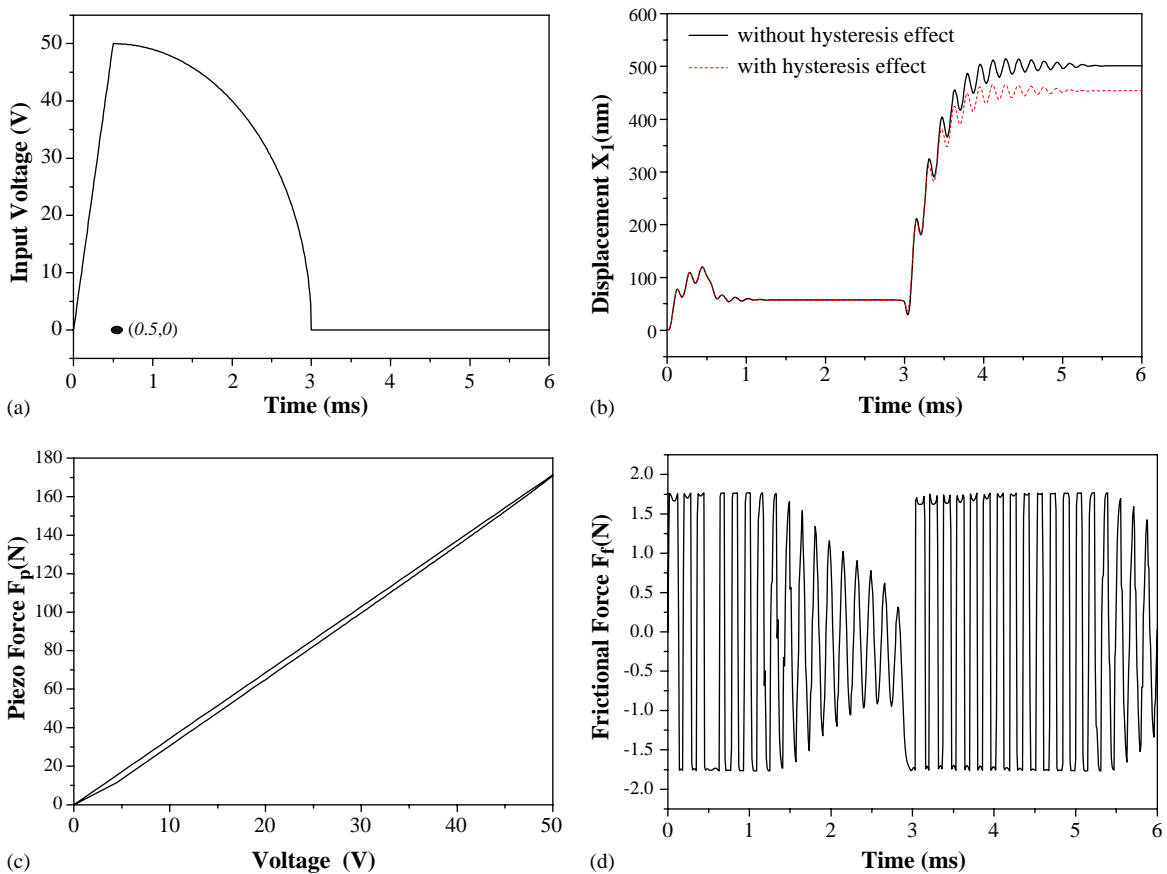

Fig. 8. Dynamic simulations of the IDM with the Bouc–Wen hysteresis model and the Leuven frictional force model: (a) the input voltage waveform; (b) displacements of the main body (—: without hysteresis effect; - - -: with hysteresis effect); (c) hysteresis phenomenon between the piezoelectric force F_p and the input voltage V; (d) frictional force F_f.
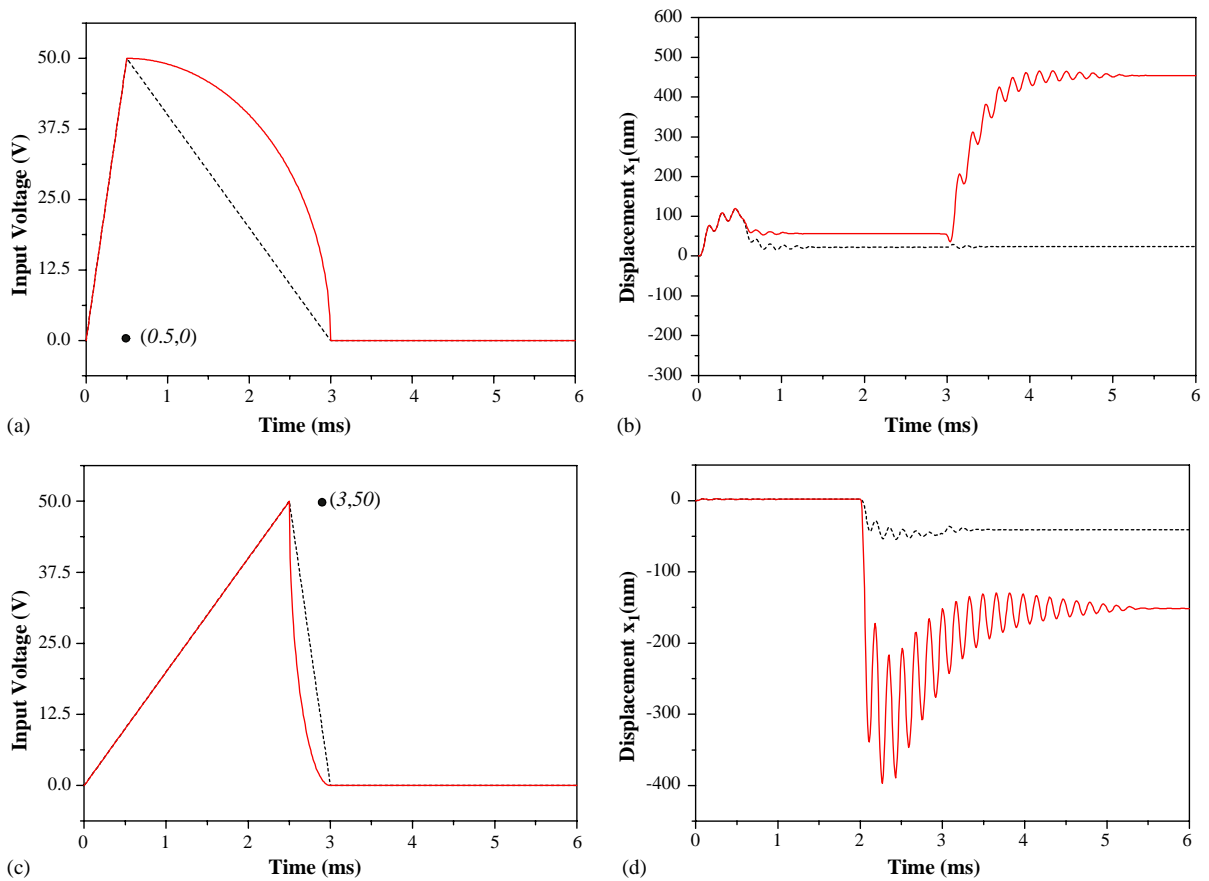
Fig. 9. Compare the main-body displacements for different shapes of the input voltage waveforms: (a) in the forward motion, the triangular input voltage waveform compares with the designed ellipse one; (b) the main-body displacements x_1 for different shapes of the input voltage waveforms; (c) In the backward motion, the triangular input voltage waveform compares with the designed ellipse one; (d) the main-body displacements for different shapes of the input voltage waveforms.

7. Feedforward compensator

As the hysteresis effect of the PE can be treated as energy dissipation, the piezoelectric force F_P is less than the original one. In Fig. 8(b), it is illustrated that the lose of piezoelectric force also makes the displacement x_1 smaller than that without hysteresis effect. Since the parameters of the Bouc–Wen hysteresis model are identified in Section 5, the effect of the hysteresis state h is well known. Therefore, the feedforward compensator [21] is employed to compensate the loss piezoelectric force F_P of the nonlinear hysteresis effect.

The flow chart of the feedforward compensation algorithm is shown in Fig. 10(a). The hysteresis effect could be compensated through the calculation of the inverse hysteresis model since the state h in Eq. (3) has identified in Section 5. The simulation results are compared in Fig. 10(b). The solid line representing the displacement x_1 with the feedforward compensator
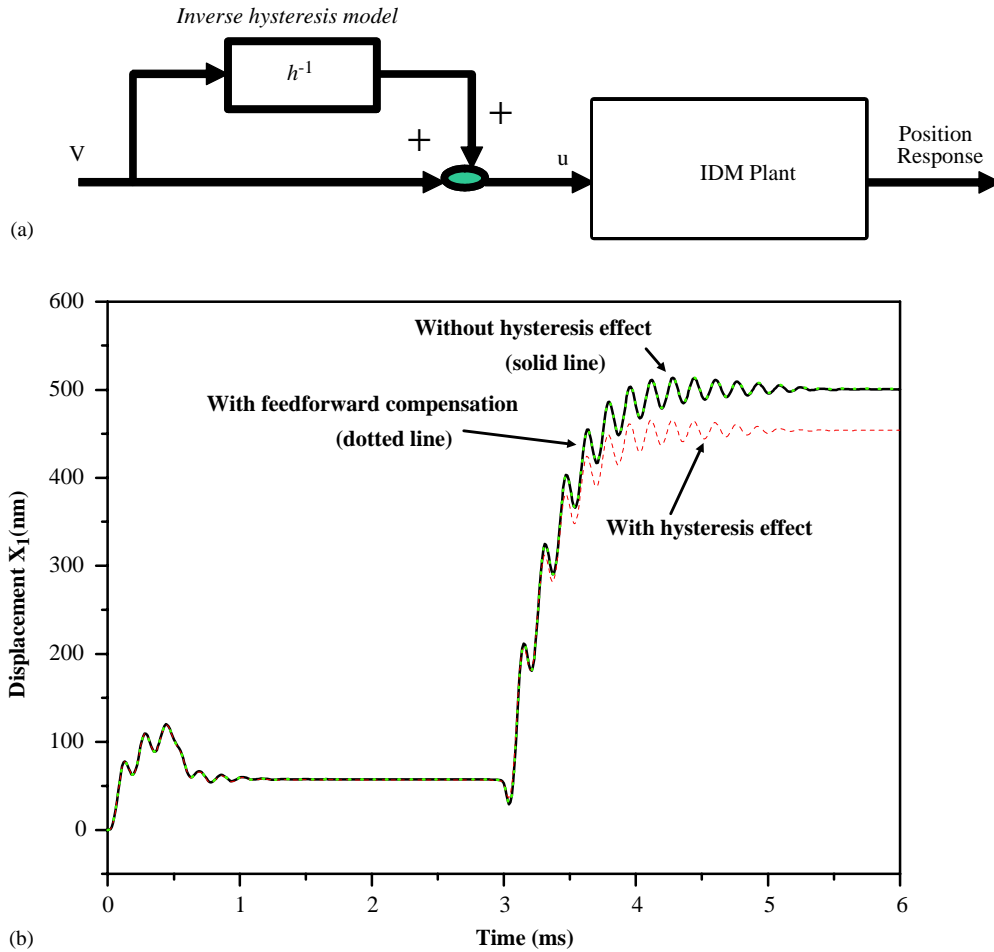
Fig. 10. Feedforward compensator to the IDM: (a) the block diagram of compensation concept; (b) the main-body displacements x_1.

coincides with the dotted line of that without the hysteresis effect in the IDM. It is found that the feedforward compensator will reduce the loss in displacements from 9.4% to 0.15%.

8. Conclusion

In this paper, the dynamic equations of the IDM with the Bouc–Wen hysteresis model and the Leuven frictional force model are formulated successfully. Additionally, with the adaptive identification method, we can confirm the characteristics of the PE and compensate the hysteresis effect by the feedforward compensator. By comparing the displacements of the main body with different shapes of the input voltage waveforms, the advantage of the new designed input voltage

waveform is assured. With all the works in this paper, the precision positioning ability of IDM will be improved.

Acknowledgements

References

[1] T. Higuchi, Application of electromagnetic impulsive force to precision positioning tools in robot system, *Second International Symposium of Robotics Research*, Kyoto, Japan, 1984, pp. 144–149.

[2] T. Higuchi, Y. Yusof, M. Watanabe, Micro actuator using recoil of an ejected mass, *IEEE Micro Robots and Teleoperators Workshops*, Massachusetts, November 9–11, Hyannis, 1987, pp. 16–21.

[3] T. Higuchi, Y. Yamagata, K. Kudoh, K. Iwasaki, Micro robot arm utilizing rapid deformation of piezoelectric elements, *Fifth International Symposium of Robotics Research*, 1989, pp. 441–448.

[4] K. Furutani, T. Higuchi, Y. Yamagata, N. Mohri, Effect of lubrication on impact drive mechanism, *Precision Engineering* 22 (1998) 78–86.

[5] Y.T. Liu, T. Higuchi, R.F. Fung, A novel precision positioning table utilizing impact force of spring-mounted piezoelectric actuator—part I: experimental design and results, *Precision Engineering* 27 (2003) 14–21.

[6] Y.T. Liu, T. Higuchi, R.F. Fung, A novel precision positioning table utilizing impact force of spring-mounted piezoelectric actuator—part II: theoretical analysis, *Precision Engineering* 27 (2003) 22–31.

[7] R.F. Fung, C.F. Han, Effects of frictional models on the dynamic responses of an impact drive mechanism, *27th Conference on Theoretical and Applied Mechanics*, Vol. I, Tainan, Taiwan, 2003, pp. 1–8.

[8] R.F. Fung, Y.T. Liu, T.K. Huang, T. Higuchi, Dynamic responses of a self-moving precision positioning stage impacted by a spring-mounted piezoelectric actuator, *Journal of Dynamic Systems, Measurement, and Control* 125 (2003) 650–661.

[9] P. Ge, M. Jouaneh, Modeling hysteresis in piezoceramic actuators, *Precision Engineering* 17 (1995) 211–221.

[10] M. Goldfarb, N. Celanovic, Modeling piezoelectric stack actuators for control of micromanipulation, *IEEE Transactions on Control Systems Technology* 17 (1997) 69–79.

[11] Y.K. Wen, Method for random vibration of hysteresis systems, *Journal of Engineering Mechanics Division* 102 (1976) 249–263.

[12] T.S. Low, W. Guo, Modeling of three-layer piezoelectric bimorph beam with hysteresis, *IEEE Journal of Microelectromechanical Systems* 4 (1995) 230–237.

[13] V. Lampaert, J. Swevers, F. Al-Bender, Modification of the leuven integrated friction model structure, *IEEE Transactions on Automation Control* 47 (2002) 683–687.

[14] M. Yar, J.K. Hammond, Parameter estimation for hysteretic system, *Journal of Sound and Vibration* 117 (1987) 161–172.

[15] X. Zhang, Y. Huang, J. Liu, X. Wang, F. Gao, A method identifying the parameters of Bouc–Wen hysteretic nonlinear model based on genetic algorithm, *Intelligent Processing Systems* (1997) 602–605.

[16] A. Kyprianou, K. Worden, Identification of hysteretic systems using differential evolution algorithm, *Journal of Sound and Vibration* 248 (2001) 289–314.

[17] A.G. Chassiakos, S.F. Masri, A.W. Smyth, T.K. Caughy, On-line identification of hysteretic systems, *Journal of Applied Mechanics* 65 (1998) 194–203.

[18] T.Y. Jiang, T.Y. Ng, K.Y. Lam, Optimization of a piezoelectric ceramic actuator, *Sensors and Actuators* 84 (2000) 81–94.

[19] Y. Hamuro, M. Yoda, S. Konishi, Acoustic impedance control system using a compact impact drive actuator, *Micromechatronics and Human Science* (2001) 99–104.
[20] M. Mita, M. Arai, S. Tensaka, D. Kobayashi, P. Basset, A. Kaiser, P. Masquelier, L. Buchaillot, D. Collard, H. Fujita, Electrostatic impact-drive microactuator, *Micro Electro Mechanical Systems* (2001) 590–593.
[21] C.J. Kempf, S. Kobayashi, Disturbance observer and feedforward design for a high-speed direct-drive positioning table, *IEEE Transactions on Control Systems Technology* 7 (5) (1999) 513–526.